Моделирование МГД волн в короне над активными областями

Leon Ofman* (CUA/NASA GSFC)

in collaboration with

Wei Liu (BAERI/LMSAL/Stanford)

*Visiting TAU

Introduction

- Coronal Seismology became possible thanks to EUV waves observations with SOHO, TRACE, SDO/AIA and other EUV instruments (Liu & Ofman2014), and was developed to study the magnetic structure of the solar corona (Nakariakov & Ofman 2001).
- SDO/AIA discovered quasi-periodic propagating fast wave trains (QPFs), with speeds of ~1000 km/s associated with flares (Liu et al. 2011; 2012), and they have been often observed in many events (e.g., Nistico et al. 2014, Liu et al. 2016).
- The fast-mode MHD wave nature of these features was confirmed by 3D MHD modeling (Ofman et al. 2011), and with 2.5D MHD models (Pascoe et al. 2013).
- The waves are associated with and provide information on eruptive and energetic events, such as flares (flare-pulsation) and CME fronts.
- Recently, it has been demonstrated that 3D MHD modeling is needed for improved coronal seismology (DeMoortel & Pascoe 2009; Ofman et al. 2015)

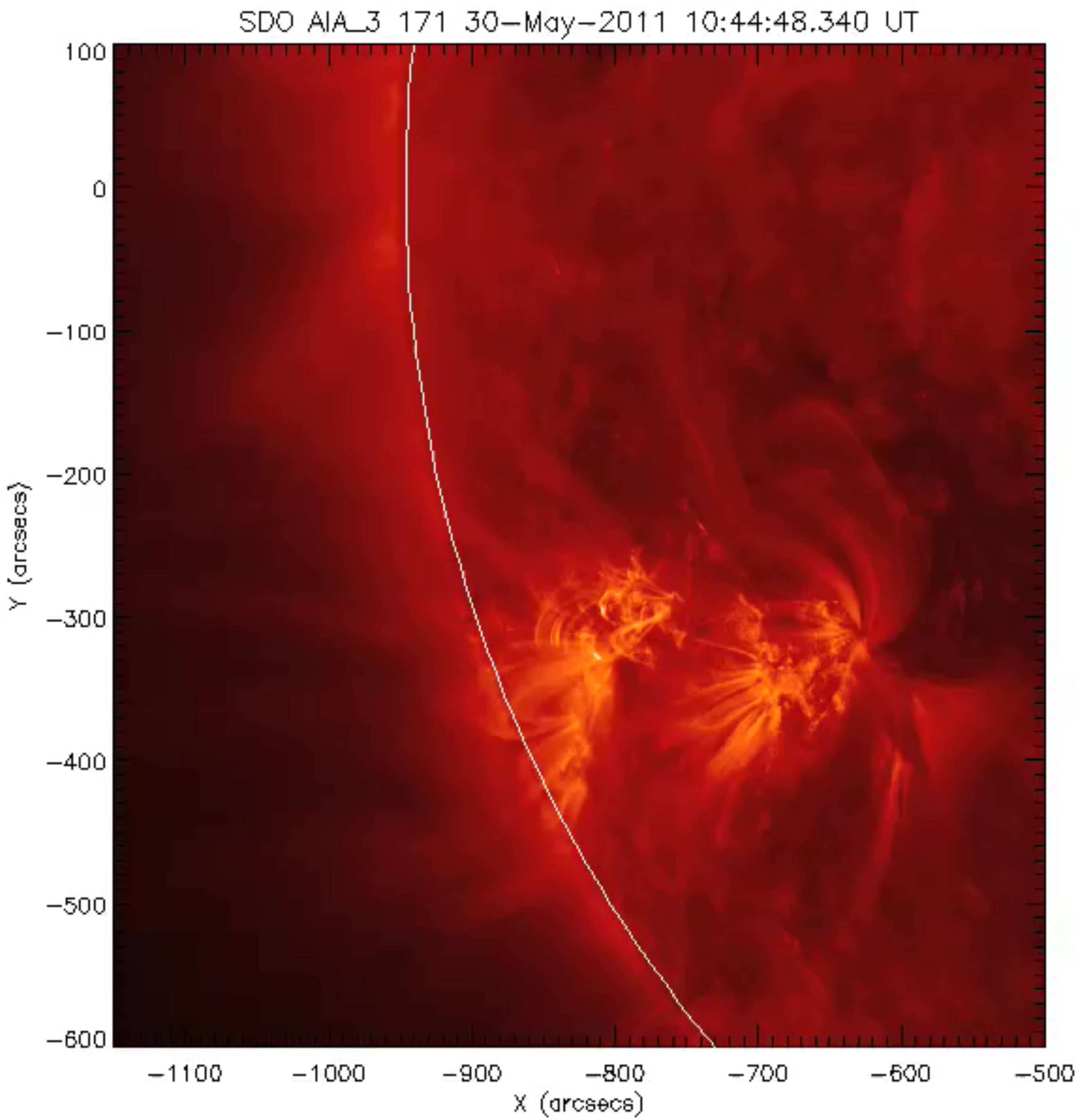
SDO AIA_3 171 30-May-2011 10:44:48.340 UT
Y (arcsecs)
X (arcsecs)
100
0
−100
−200
−300
−400
−500
−600
−1100
−1000
−900
−800
−700
−600
−500

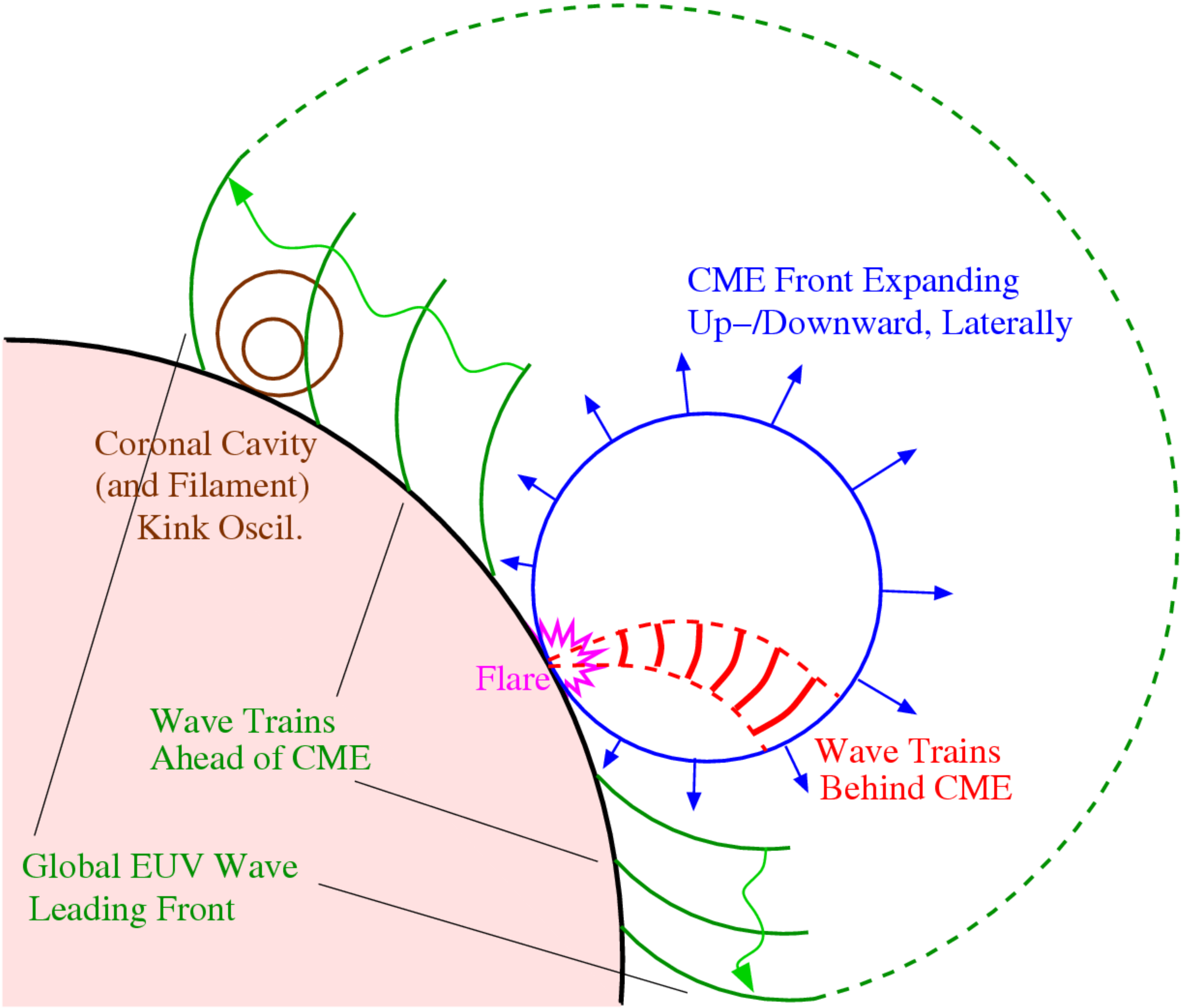

Schematic view of an EUV wave event, showing quasi-periodic wave trains running ahead of (green) and behind (red) the CME front (blue)

From: Wei Liu

Observations: flare-driven QFPs

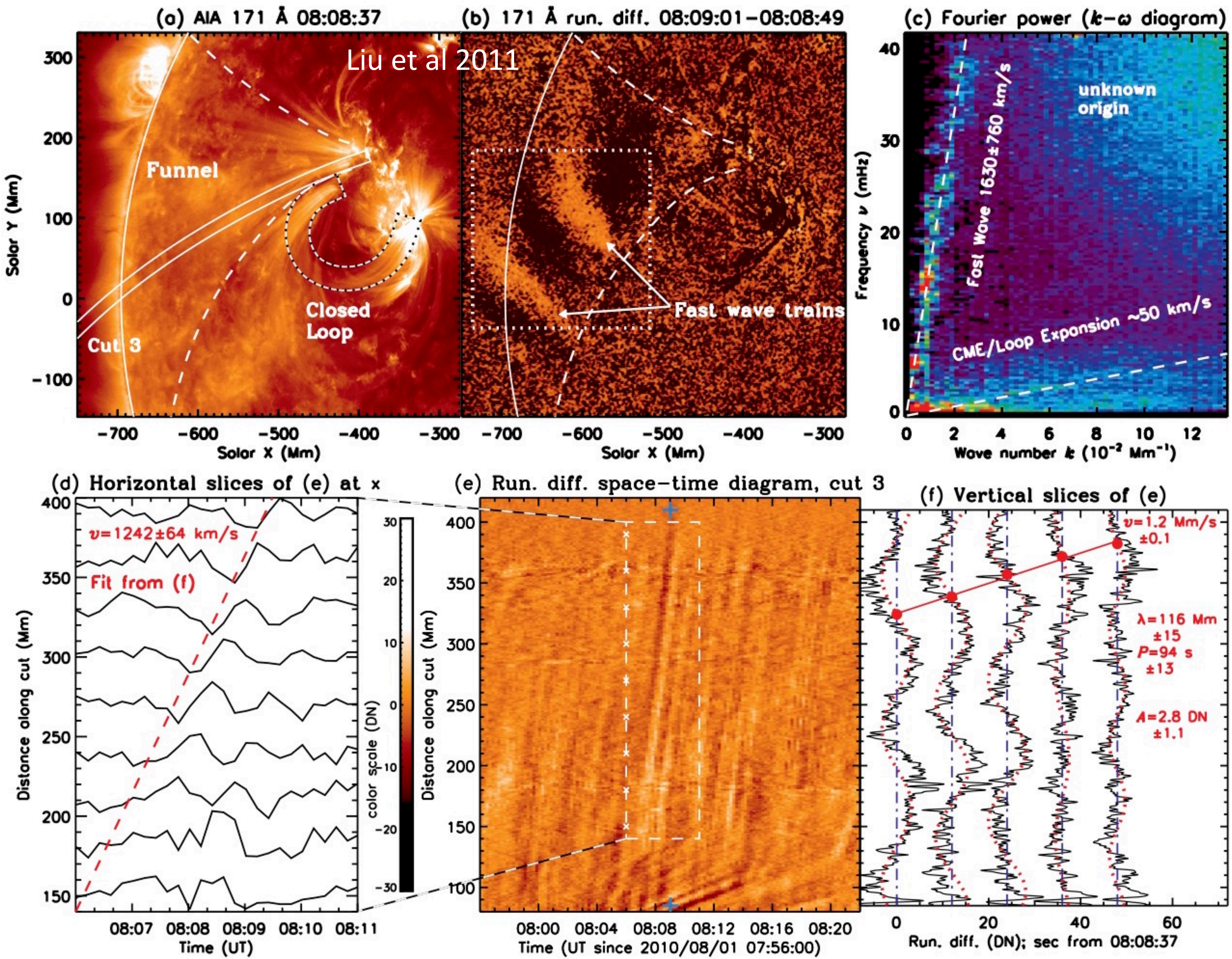

Correlation between flare and wave pulsations

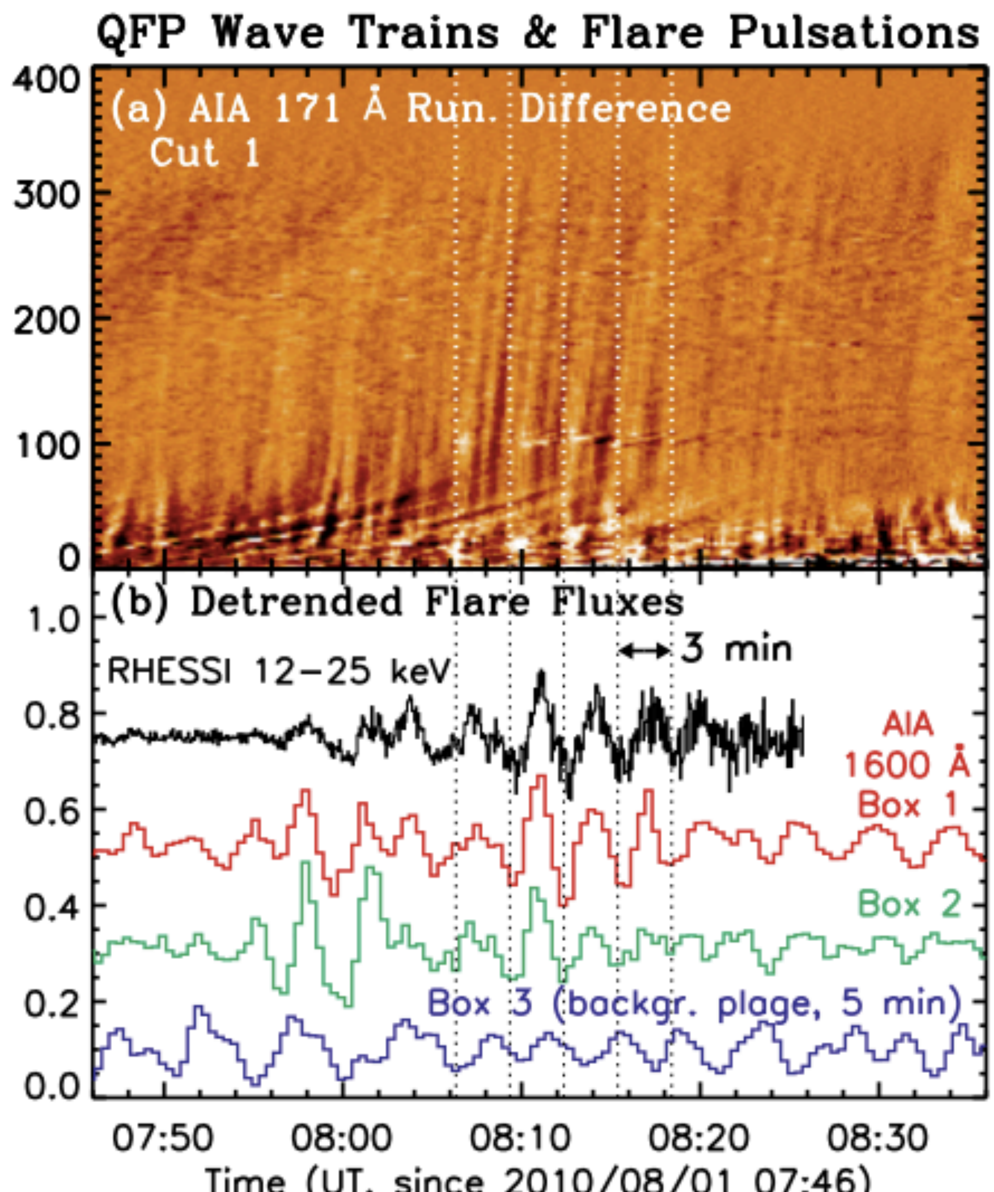

Observations: statistics and DEM

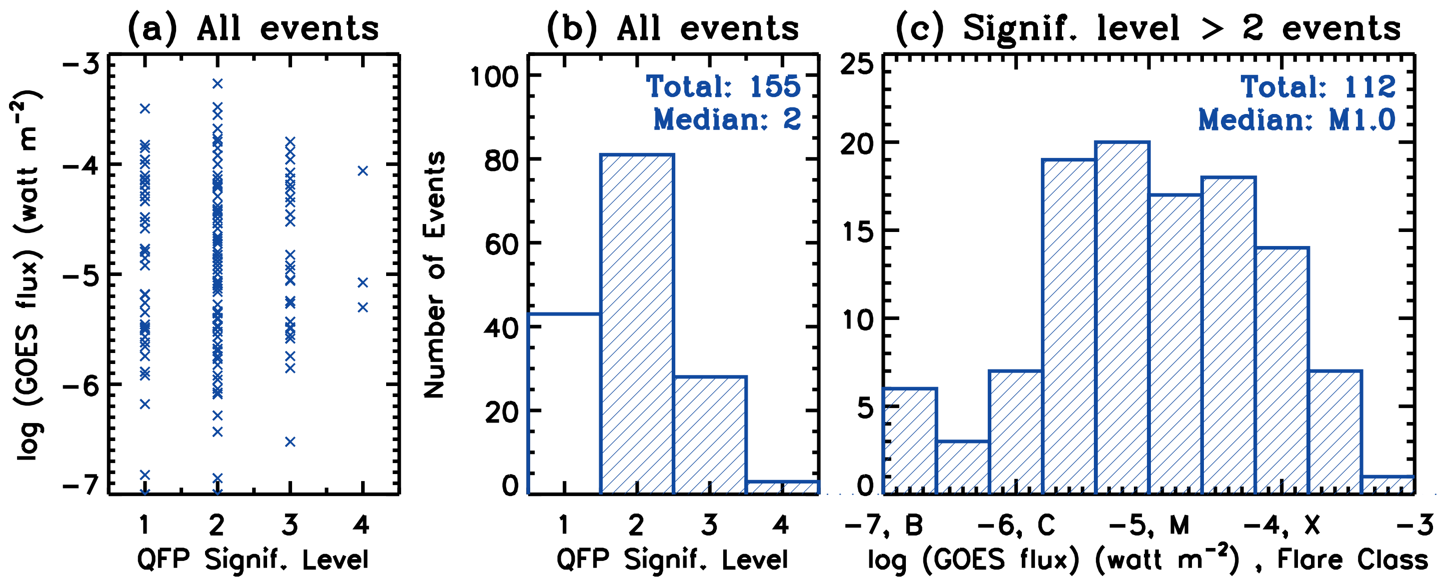

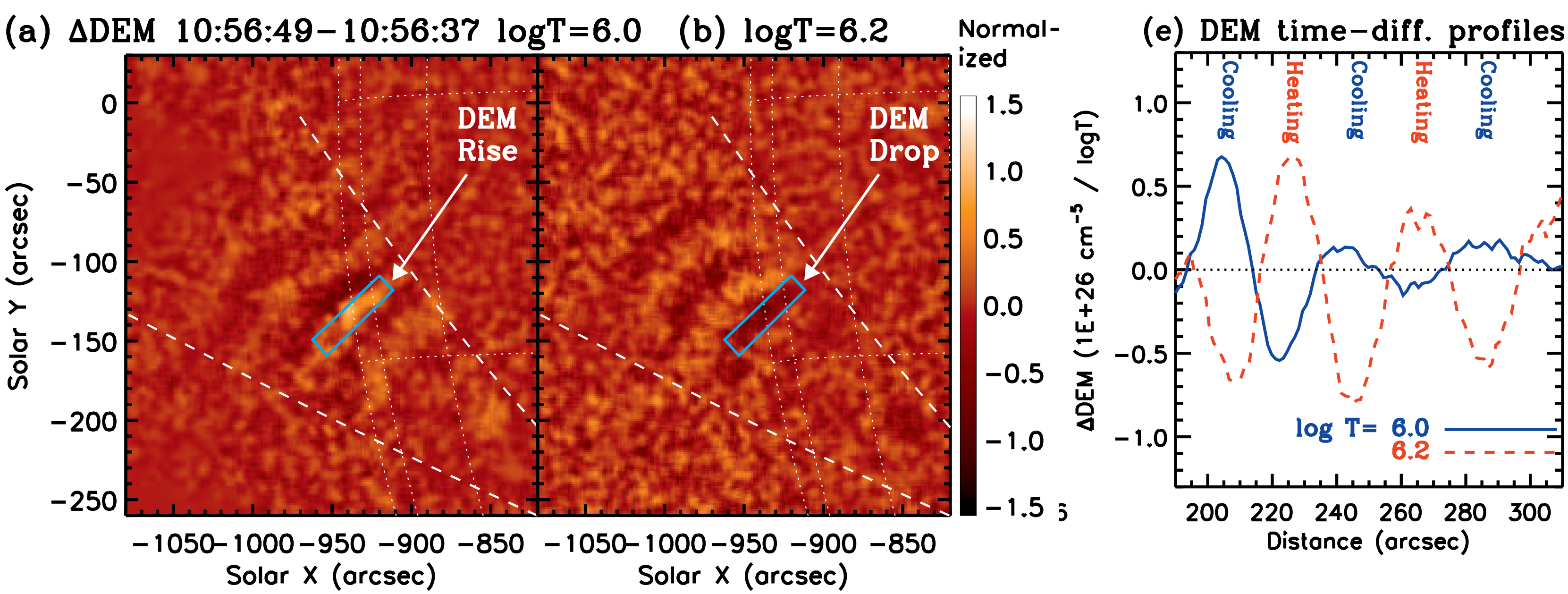

QPF waves coronal seismology (CS)

- Detection of phase speed (example: $v_{ph}=2200\pm130\ km\ s^{-1}$)=> determine B from V_{ph}; need *n, T* (example: $B = v_{ph}(4\pi\rho)^{0.5}=8G$ within 50%)
- Detection of wavelength => *T, n, B* (example: *T=0.8-1MK* for 1-Aug-2010 event)
- Detection of location/direction/shape => determine 3D magnetic structure consistency
- Oscillations period/amplitude => flare oscillations, flare energy release properties (example: energy flux $\rho v^2 V_{ph}/2 =(0.1–2.6)x10^7\ erg\ cm^{-2}\ s^{-1}$)
- Damping/dissipation => magnetic field divergence/thermal, viscous, resistive coefficients
- Complication: wave properties depend on 3D magnetic and phase speed structure => 3D MHD modeling with parameterized realistic AR structure => model parameter fitting for improved CS

Coronal seismology based on linear wave dispersion

- Sausage (|B|, ρ)
- Kink (almost incompressible)
- Torsional (incompressible)
- Magneto-acoustic (ρ, V)

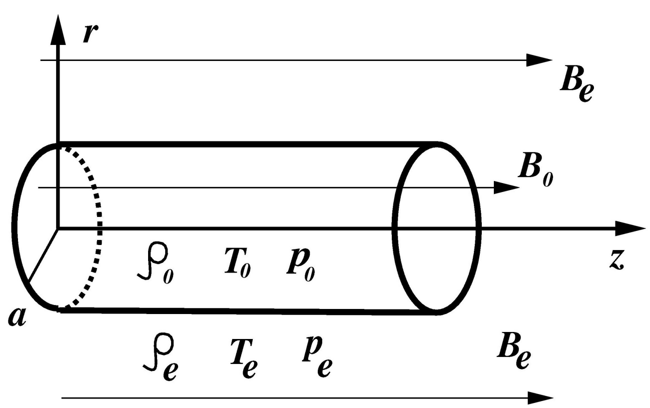

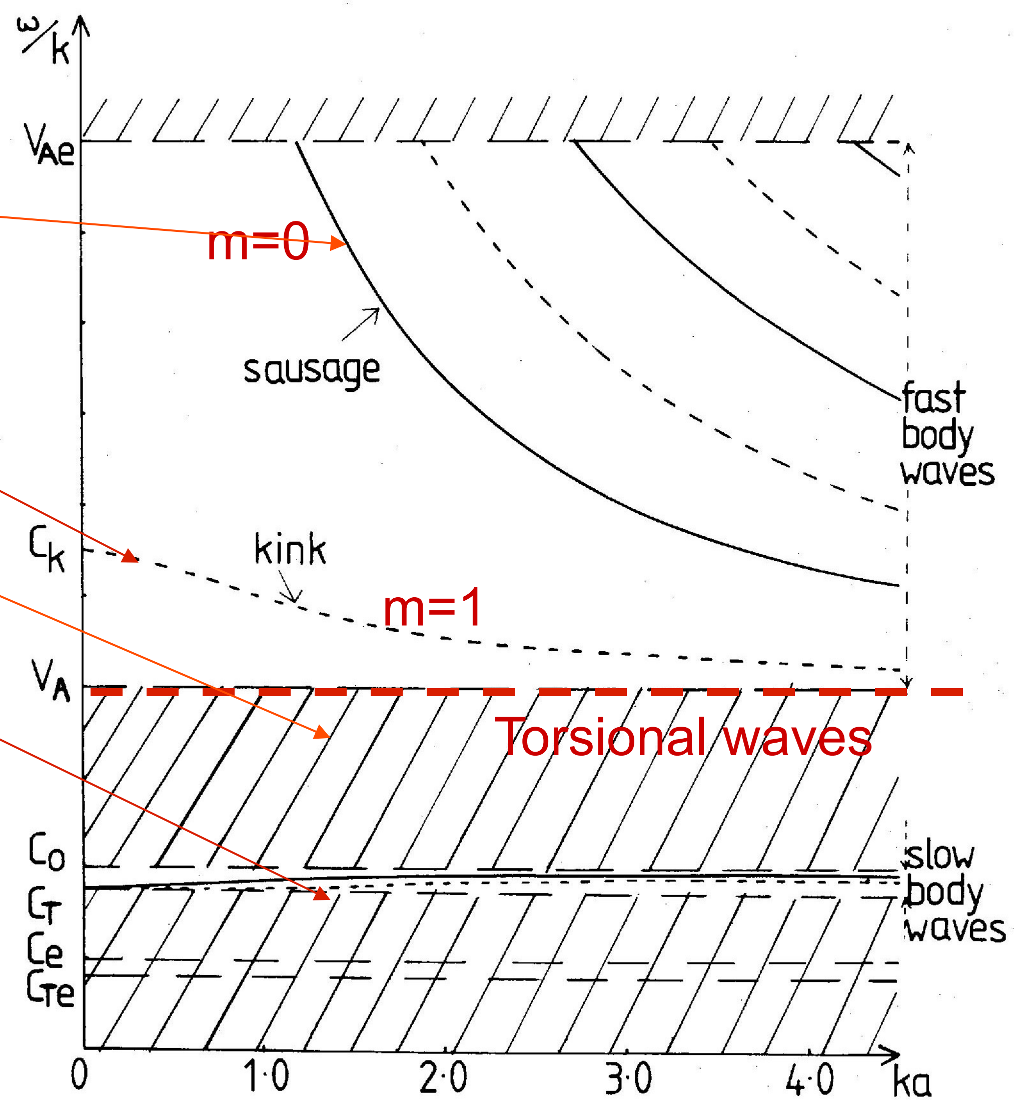

Roberts 1981:

From V. M. Nakariakov

Modeling waves in AR

- Dipole magnetic field (white curves) used for the model AR.
- The field strength decreases rapidly with height.
- Gravitationally stratified density
- The intensity scale shows the magnetic field magnitude at the base of the AR.
- Dimensionless units.

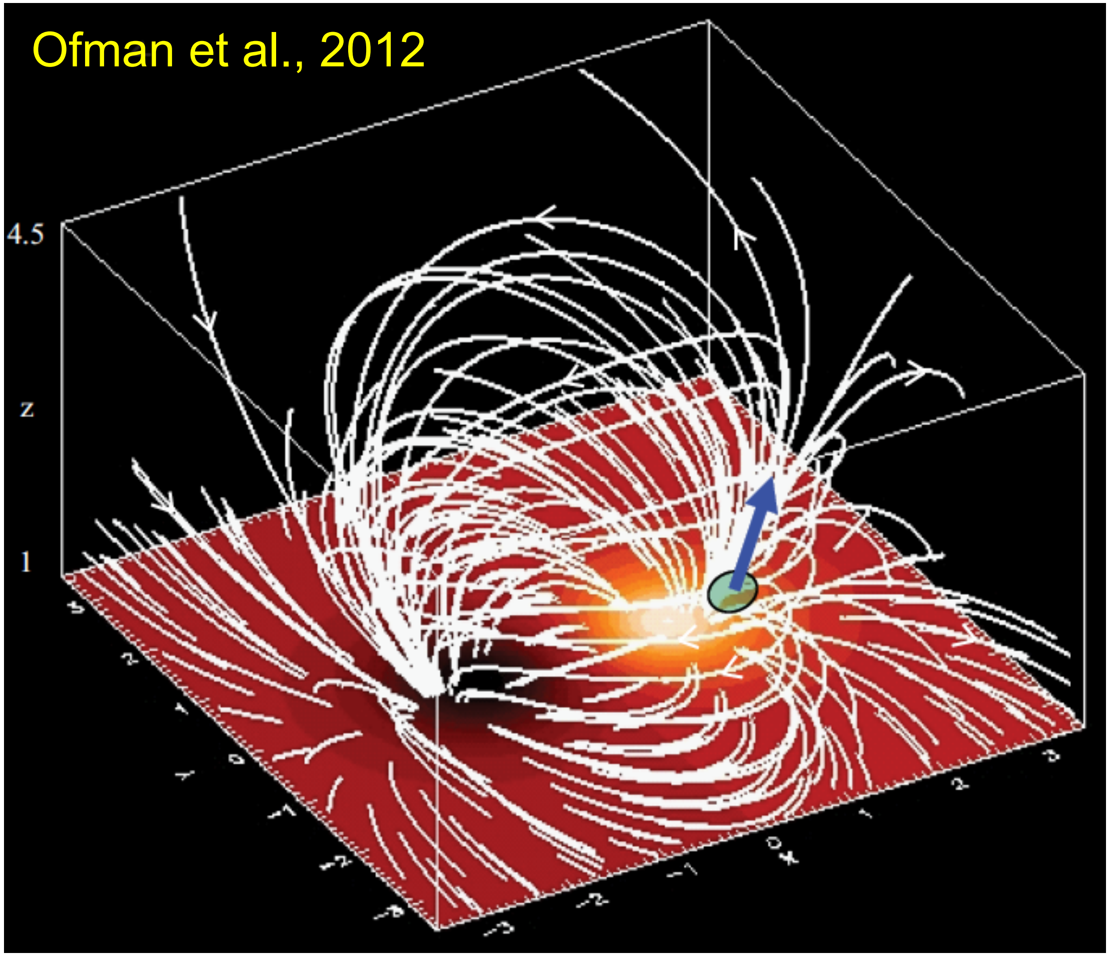

Slow waves excitation by flows along the field:

$$\mathbf{V} = V_0(x, y, z = z_{min}, t)\mathbf{B}/|B|,$$

Driven fast magnetosonic waves:

$\mathbf{V}=V_0\ \mathbf{e_x}$, where

$$V_0(x, y, z = z_{min}, t) = A_v(t)V_A exp\left\{-\left[\left(\frac{x-x_0}{w_0}\right)^2 + \left(\frac{y-y_0}{w_0}\right)^2\right]^2\right\},$$

$A_v(t)=\sin(\omega t)$

Polytropic MHD equations

Continuity: $$\frac{\partial \rho}{\partial t} + \nabla \cdot \left(\rho \vec{V} \right) = 0,$$

Momentum: $$\rho \left[\frac{\partial \vec{V}}{\partial t} + \left(\vec{V} \cdot \nabla \right) \vec{V} \right] = -\nabla p - \frac{G M_S \rho}{r^2} + \frac{1}{c} \vec{J} \times \vec{B} + \vec{F}_v,$$

Inductance (Faraday): $$\frac{\partial \vec{B}}{\partial t} = -c \nabla \times \vec{E}, \;\; \vec{E} = -\frac{1}{c} \vec{V} \times \vec{B} + \eta \vec{J},$$

Current (Amper's law): $$\nabla \times \vec{B} = \frac{4\pi}{c} \vec{J},$$

Energy (Temperature): $$\frac{\partial T}{\partial t} = -(\gamma - 1) T \nabla \cdot \vec{V} - \vec{V} \cdot \nabla T + (\gamma - 1)(S_{heat} - S_{loss}),$$

Polytropic index: $$1 \le \gamma \le 5/3$$

3D MHD Model Equations

$$\frac{\partial \rho}{\partial t} + \nabla(\rho \mathbf{V}) = 0, \tag{i}$$

$$\frac{\partial(\rho \mathbf{V})}{\partial t} + \nabla \cdot \left[\rho \mathbf{V}\mathbf{V} + \left(E_u p + \frac{\mathbf{B}\cdot\mathbf{B}}{2}\right)\mathbf{I} - \mathbf{B}\mathbf{B}\right] = -\frac{1}{F_r}\rho \mathbf{F}_g \tag{ii}$$

$$\frac{\partial(\rho E)}{\partial t} + \nabla \cdot \left[\mathbf{V}\left(\rho E + E_u p + \frac{\mathbf{B}\cdot\mathbf{B}}{2}\right) - \mathbf{B}(\mathbf{B}\cdot\mathbf{V}) + \frac{1}{S}\nabla \times \mathbf{B} \times \mathbf{B}\right] =$$

$$= \frac{1}{F_r}\rho \mathbf{F}_g \cdot \mathbf{V} - n^2\Lambda(T) + \nabla_{||}\cdot(\kappa_{||}\nabla_{||}T) + H_{in}, \tag{iii}$$

$$\frac{\partial \mathbf{B}}{\partial t} = \nabla \times (\mathbf{V} \times \mathbf{B}) + \frac{1}{S}\nabla^2 \mathbf{B}. \tag{iv}$$

Total energy density: $\rho E = \frac{p}{(\gamma-1)} + \frac{\rho V^2}{2} + \frac{B^2}{2}$, adiabatic index $\gamma = 5/3$ (for empirical polytropic models use $\gamma = 1.05$ without heat conduction), Euler number $E_u = \beta/2$, Froude number $F_r = V_A^2 L_0/GM_s$, Lundquist number $S = L_0 V_A/\eta$, the Alfvén speed $V_A = B_0/\sqrt{4\pi\rho}$, $n = \rho/m_p$, $\Lambda(T)$ is the optically thin radiative loss function, H is the empirical heating function, $\nabla_{||} = \frac{\mathbf{B}}{|\mathbf{B}|}\cdot\nabla$, and $\kappa_{||}$ is the parallel to $\mathbf{B}$ heat conduction coefficient.

Initial and boundary conditions

- Dipole magnetic field (as in Ofman and Thompson 2002; Ofman et al. 2015)
- Hydrostatic density: $\boxed{\rho = \rho_0 e^{[1/(10+z-z_{min})-0.1]/H}}$ where $\boxed{H = 2k_B T_0 R_s/(10 G M_s m_p)}$
- Fast magnetosonic speed V_f; plasma $\beta=8\pi nkT/B^2=2C_s^2/V_A^2$
- Boundary conditions: line tied at z=1, open at other 5 planes.

B_0=100G
T_0=1MK
N_0=1.4e9 cm^{-3}

The initial bipolar magnetic field of the model AR

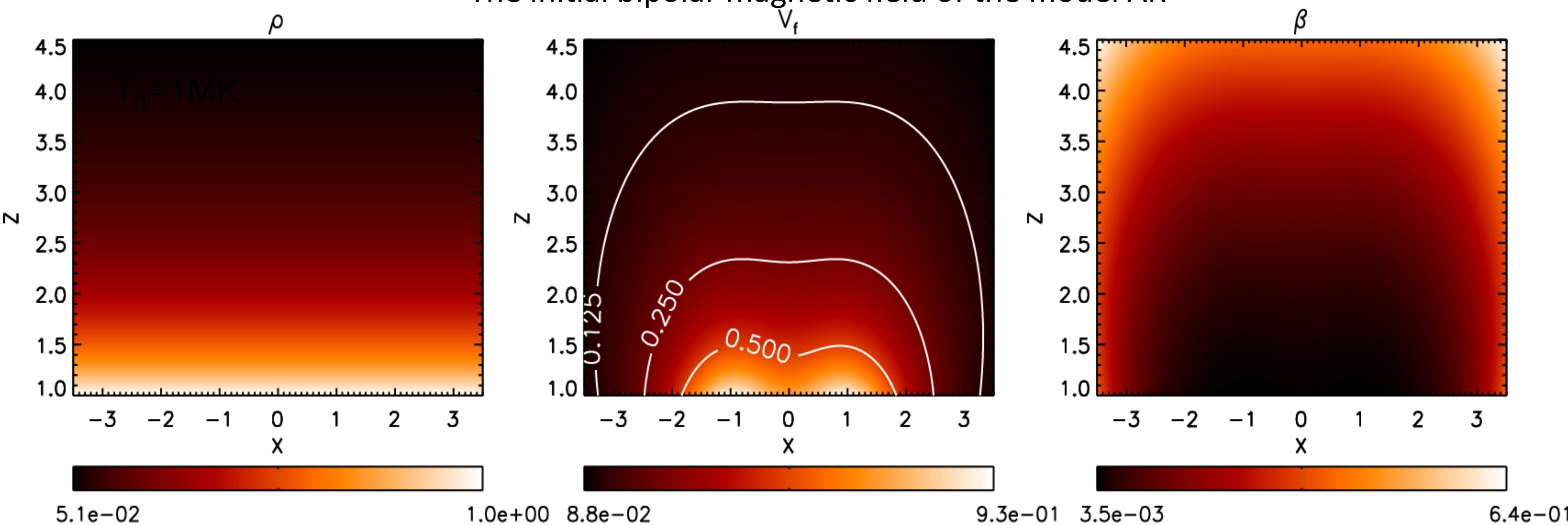

The initial density (left), fast magnetosonic speed (middle), and plasma in the *xz* plane at t=0 in the model AR. The contours on V_f show the 50%, 25%, and 12.5% levels of the maximal value.

Typical resolution: 256^3 to 512^3; MPI parallel code solved on 256 to 512 processors.

3D structure of wave density perturbation

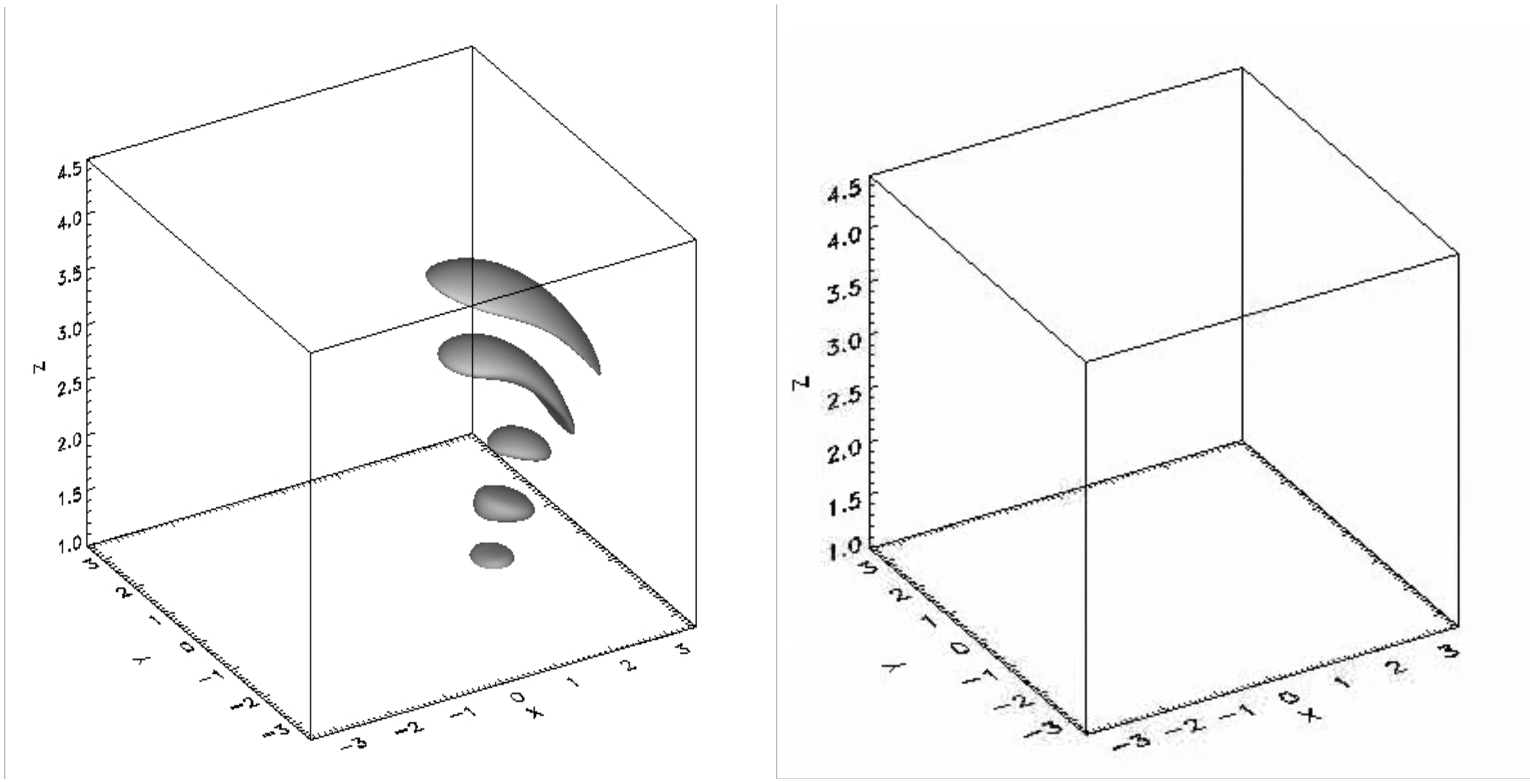

The three dimensional density perturbation structure due to the driven fast magnetosonic waves shown as an isosurface (at the level n_s=0.015) at t=22, 38 τ_A demonstrating the propagation of the fast magnetosonic wave in the magnetic 'funnel' produced by the structure of the background dipolar magnetic field and the gravitationally stratified density.

Deflection of magnetic field lines by the waves

V_{x0}=0.02

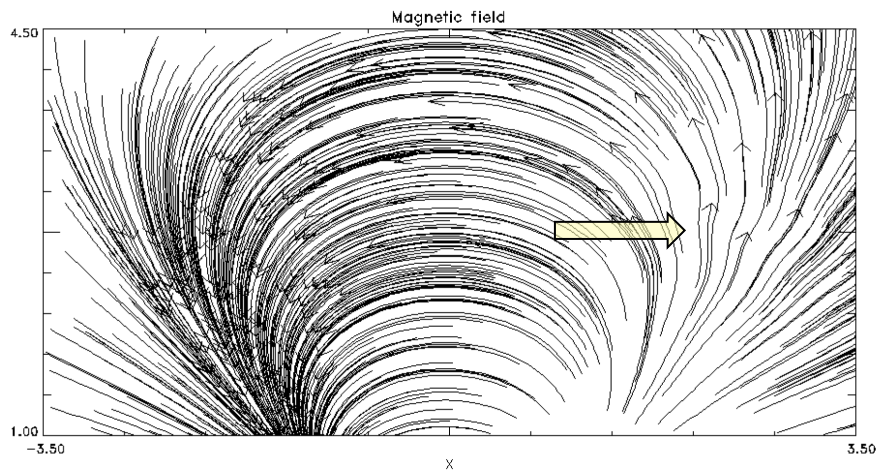

V_{x0}=0.1

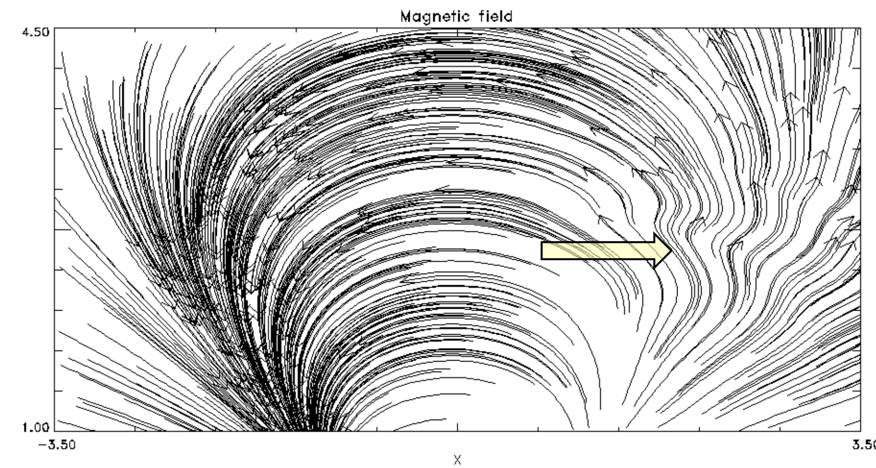

Magnetic field lines of the model active region in the *x-z* plane. Left panel shows the fast magnetosonic waves in the magnetic 'funnel' (arrow) for driving velocity amplitude $V_{x0}=0.02V_A$ The right panel is for large $V_{x0}=0.1V_A$ to demonstrate more clearly the effects of the waves on the magnetic field.

Propagating wavefronts and time dependence of the components

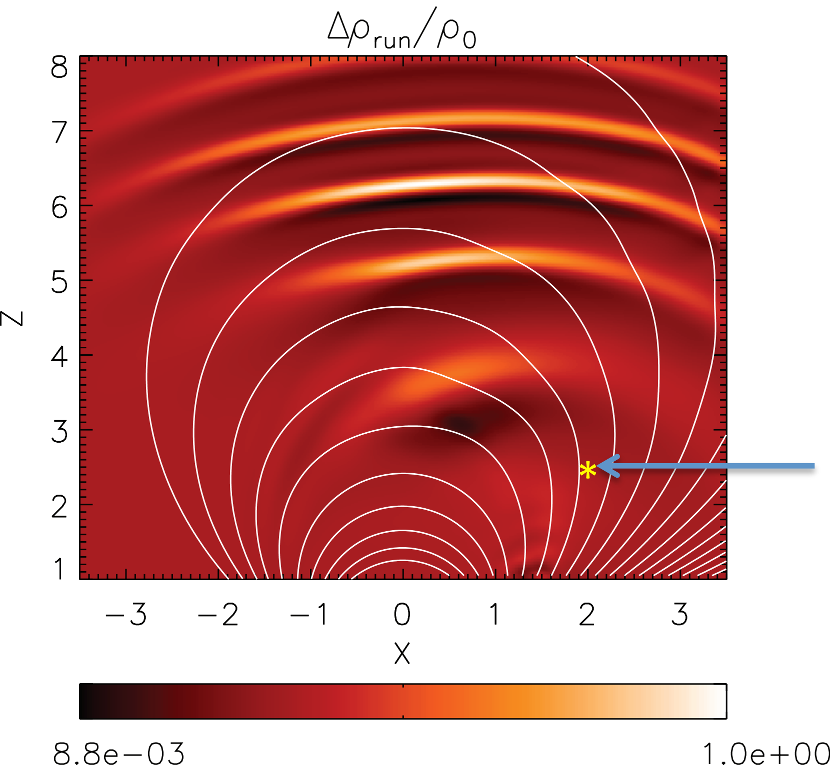

Density running difference (normalized by the initial value) and magnetic field lines in the xz-plane at the center of the AR (y = 0). Density perturbations due to QFPs launched at the bottom boundary are evident and similar to those in AIA images.

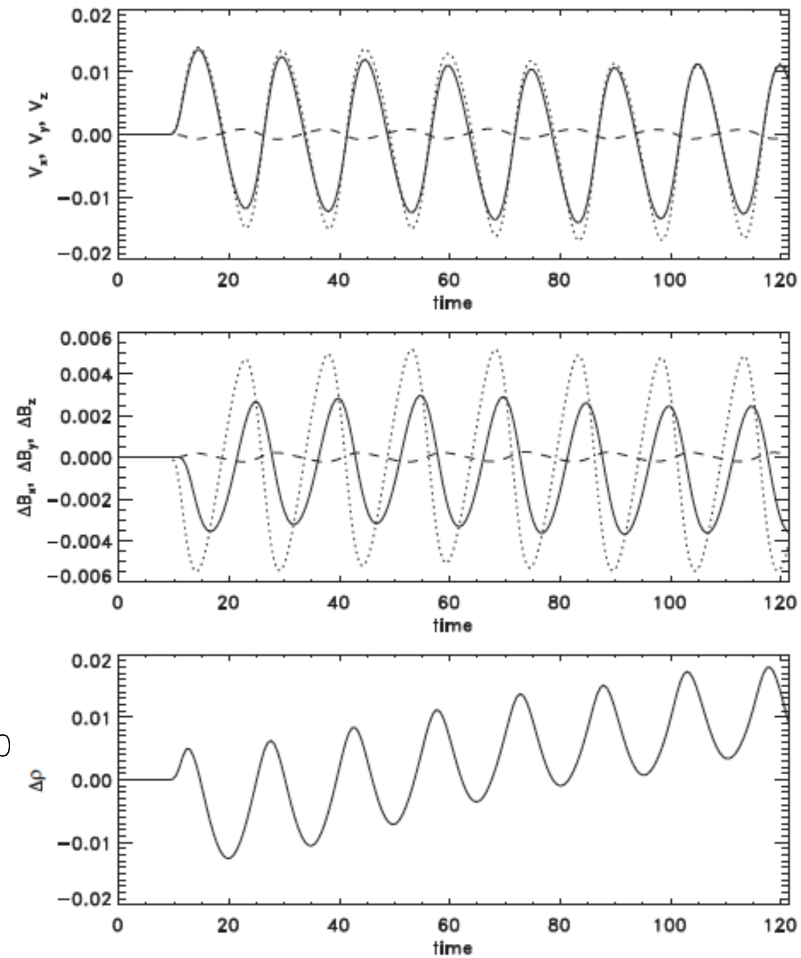

The temporal evolution of the velocity components at a point.

The perturbed magnetic field components.

The density perturbation.

Modeling fast quasi-periodic MHD waves in AR magnetic funnels

Liu et al 2011; Ofman et al 2011

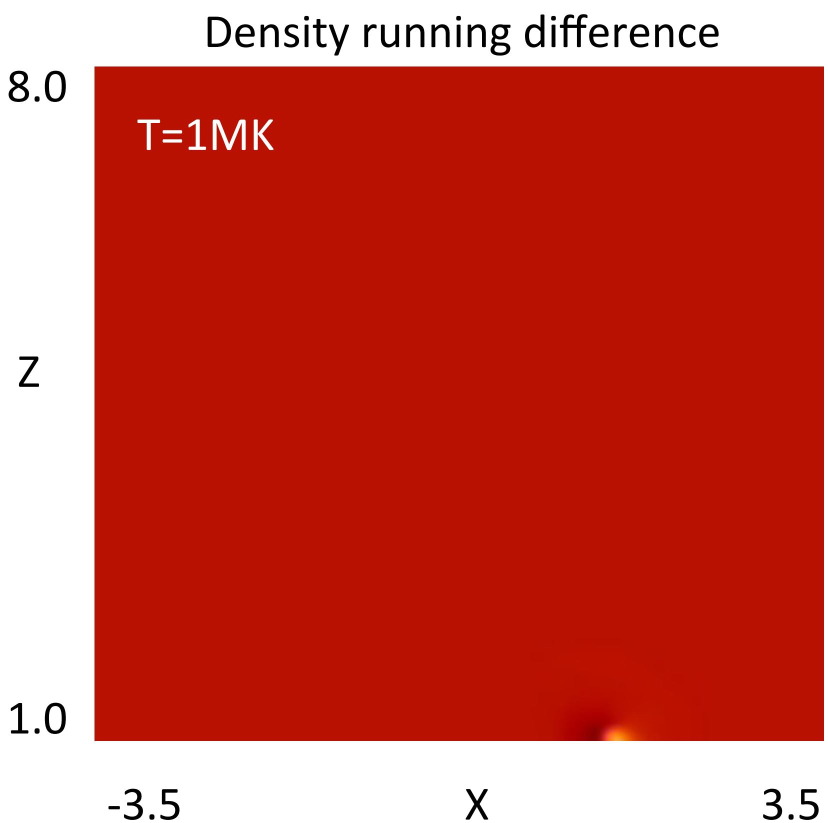

Phase speed: 1000-2000 km/s

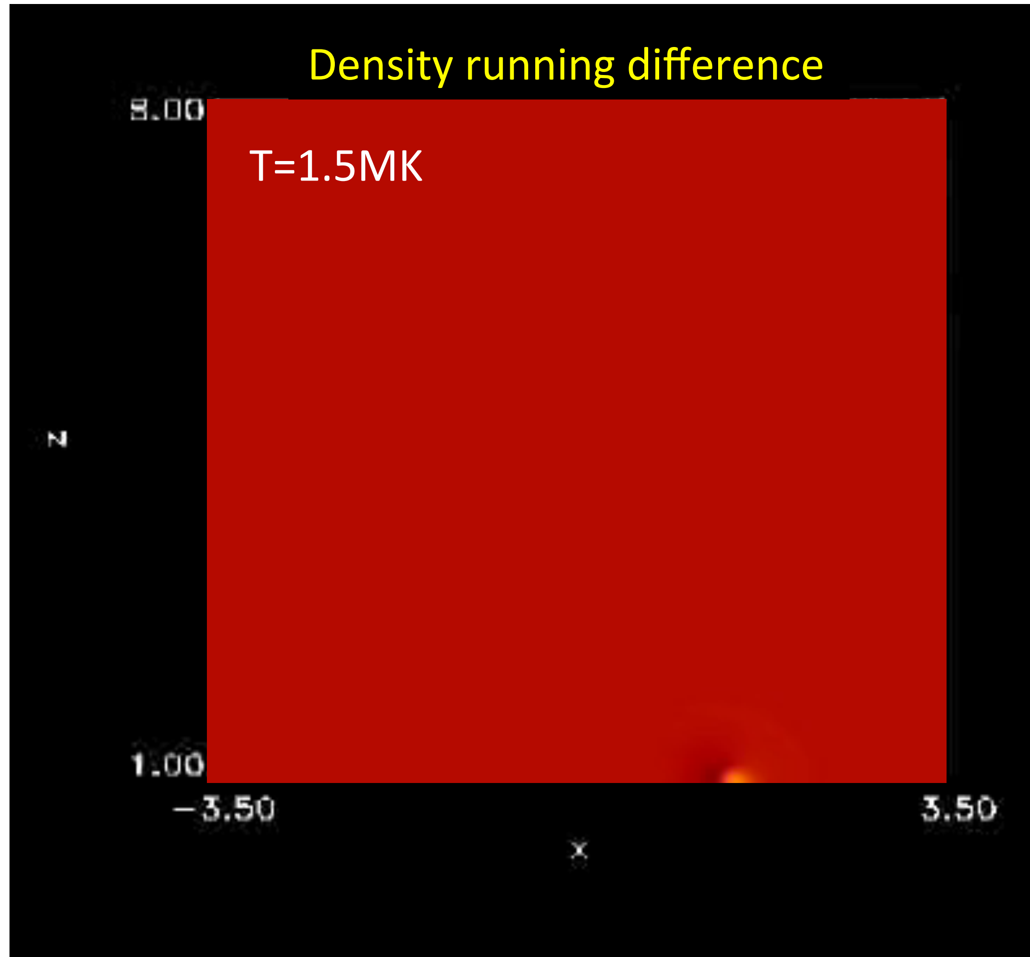

B_0=100G; N_0=1.4e9 cm^{-3}

Energy flux: $(0.1–2.6)\ x10^7\ erg\ cm^{-2}\ s^{-1}$

Single source vs. counter propagating QPFs

One wave source

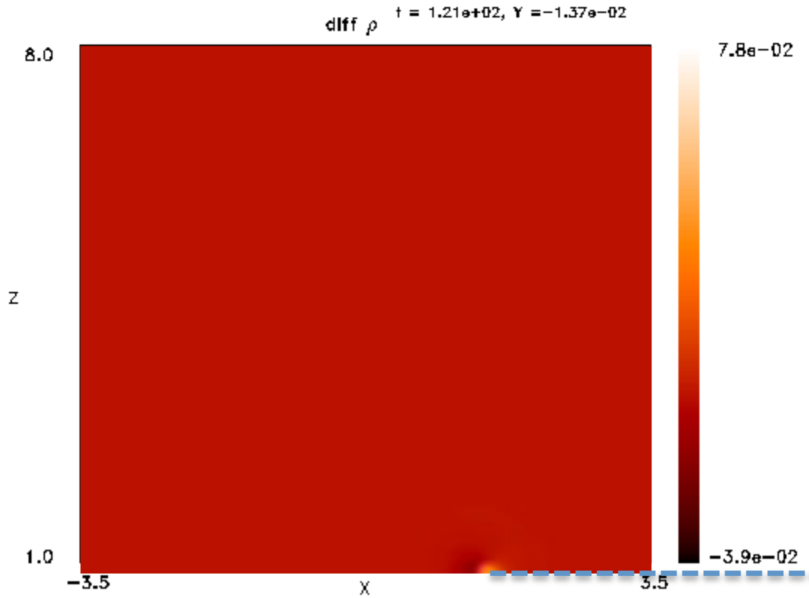

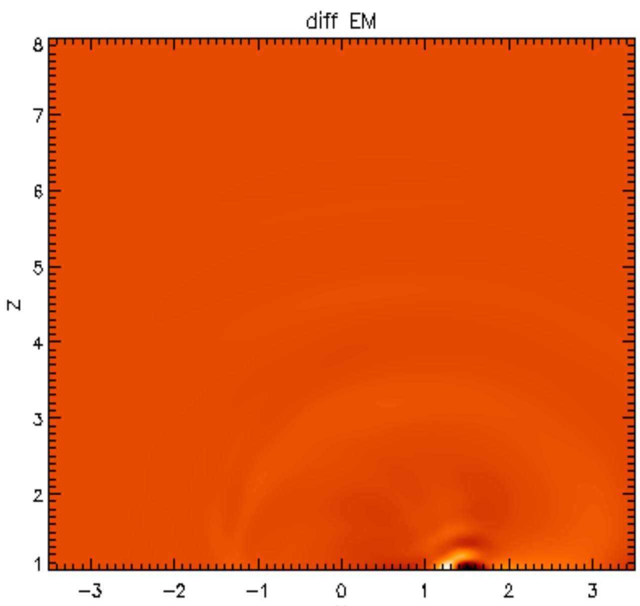

Two counter-propagating waves sources

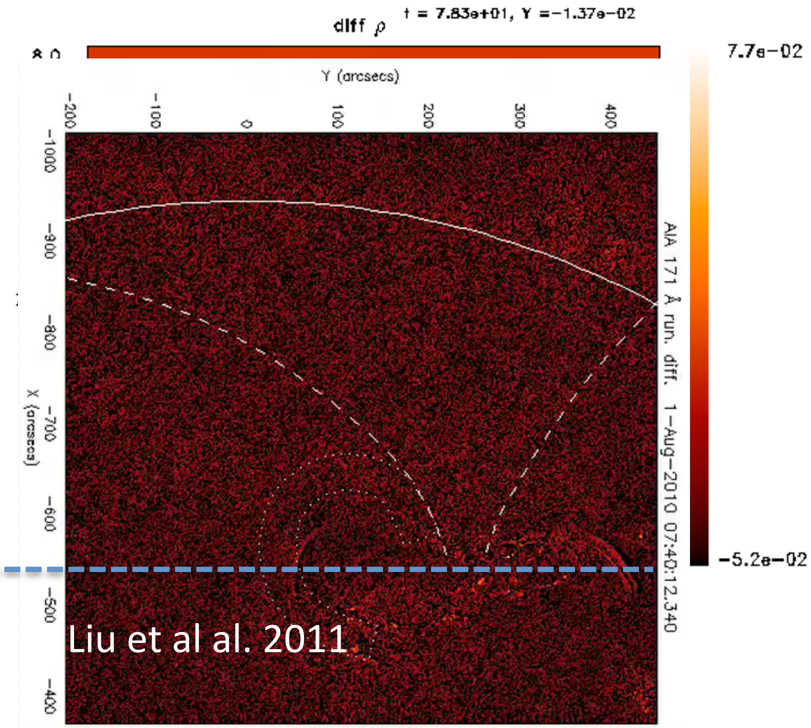

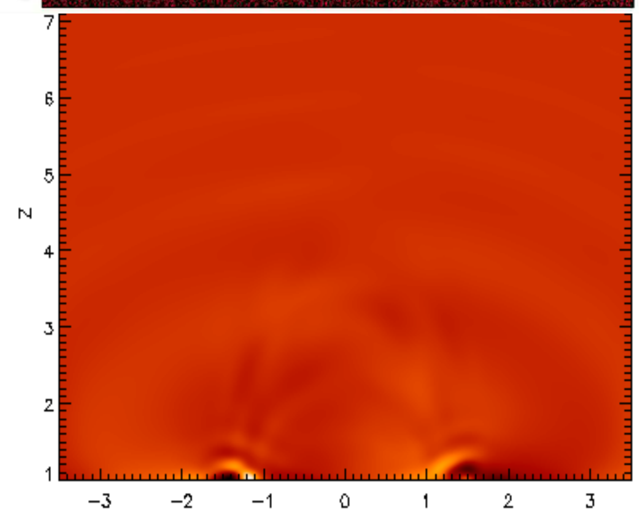

Single source vs. counter propagating QPFs

One wave source

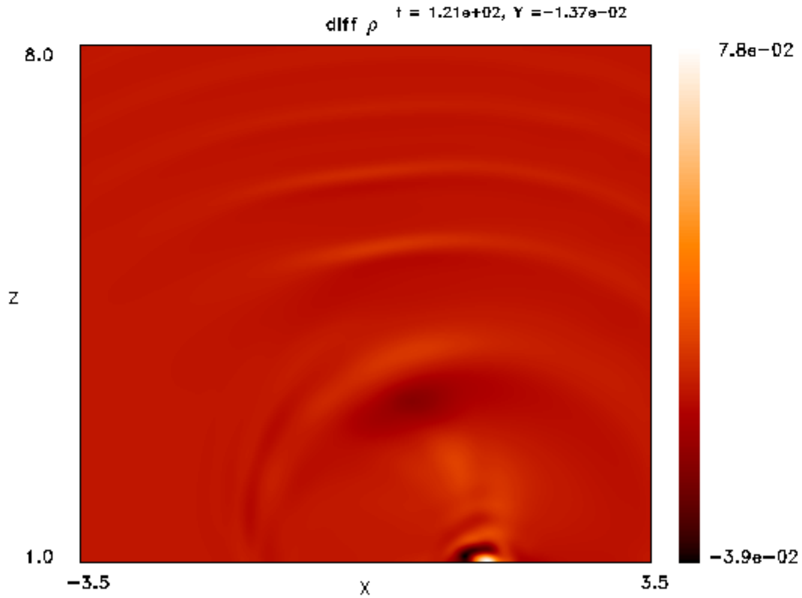

Two counter-propagating waves sources

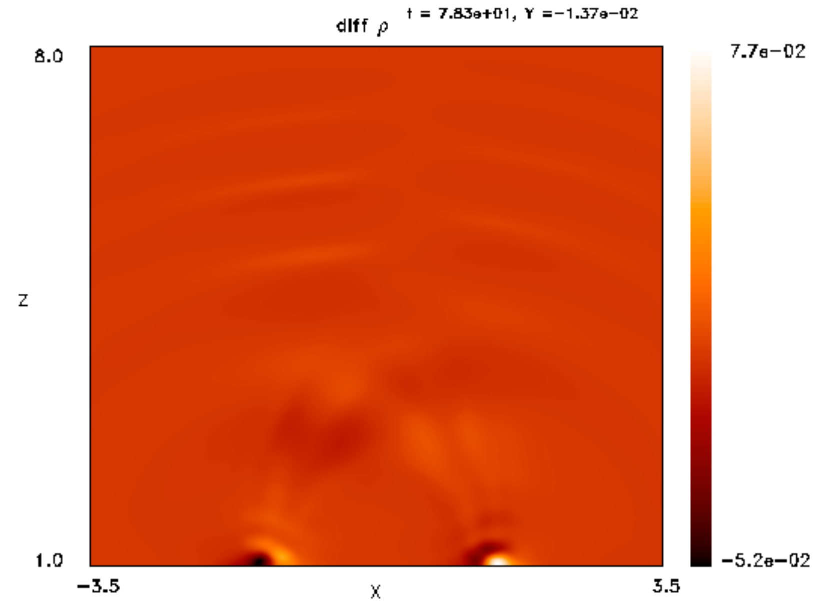

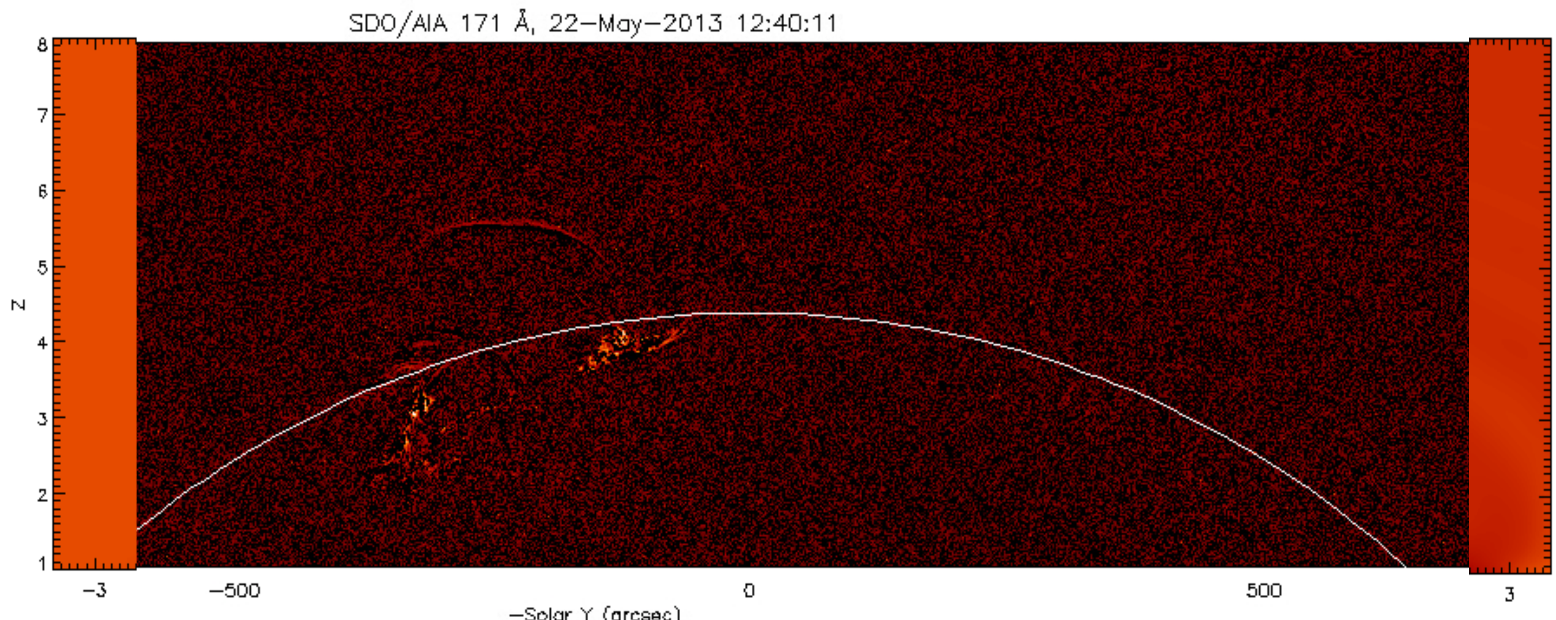

On-limb view of QPF waves

- On limb view => 3D structure of the AR field
- Oscillating bright points (e.g., Ugarte-Urra et al. 2004; Doyle et al. 2006; Tian et al. 2008; Tanmoy et al. 2016)?

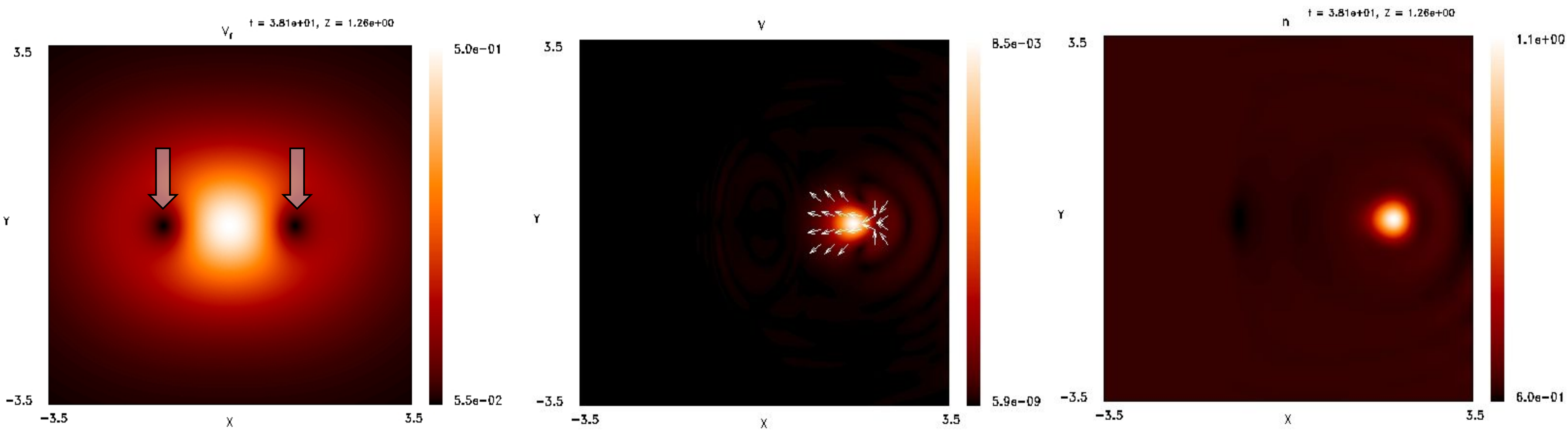

The cut in the *x-y* plane at *z=1.26* of the fast magentosonic speed V_f (left), the velocity (middle), and the density (right) due to the waves at $t=38.1\ \tau_A$. The low V_f in the regions marked by the arrows lead to trapping of the fast magnetosonic waves.

τ_A=11.9s

Transverse Loop arcade oscillations

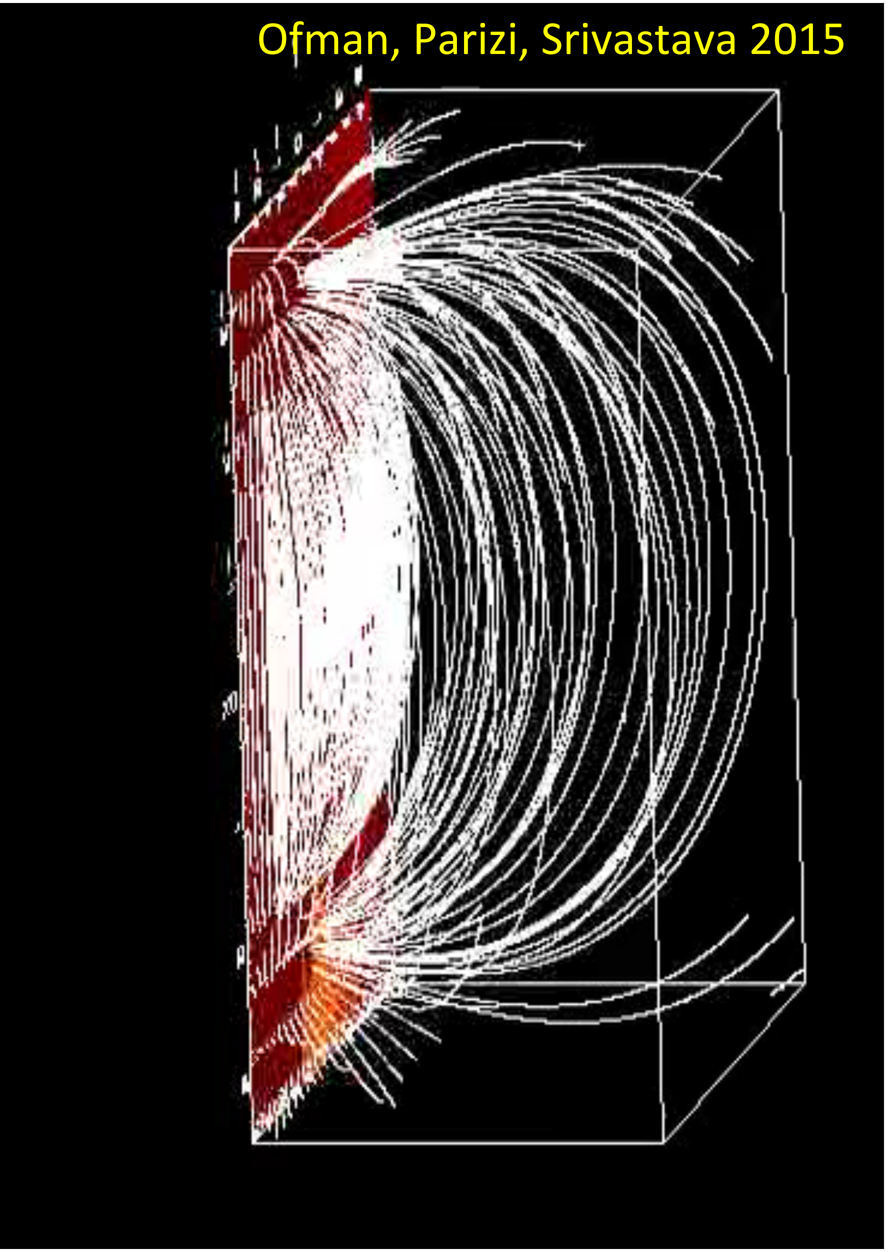

Srivastava & Goossens 2013

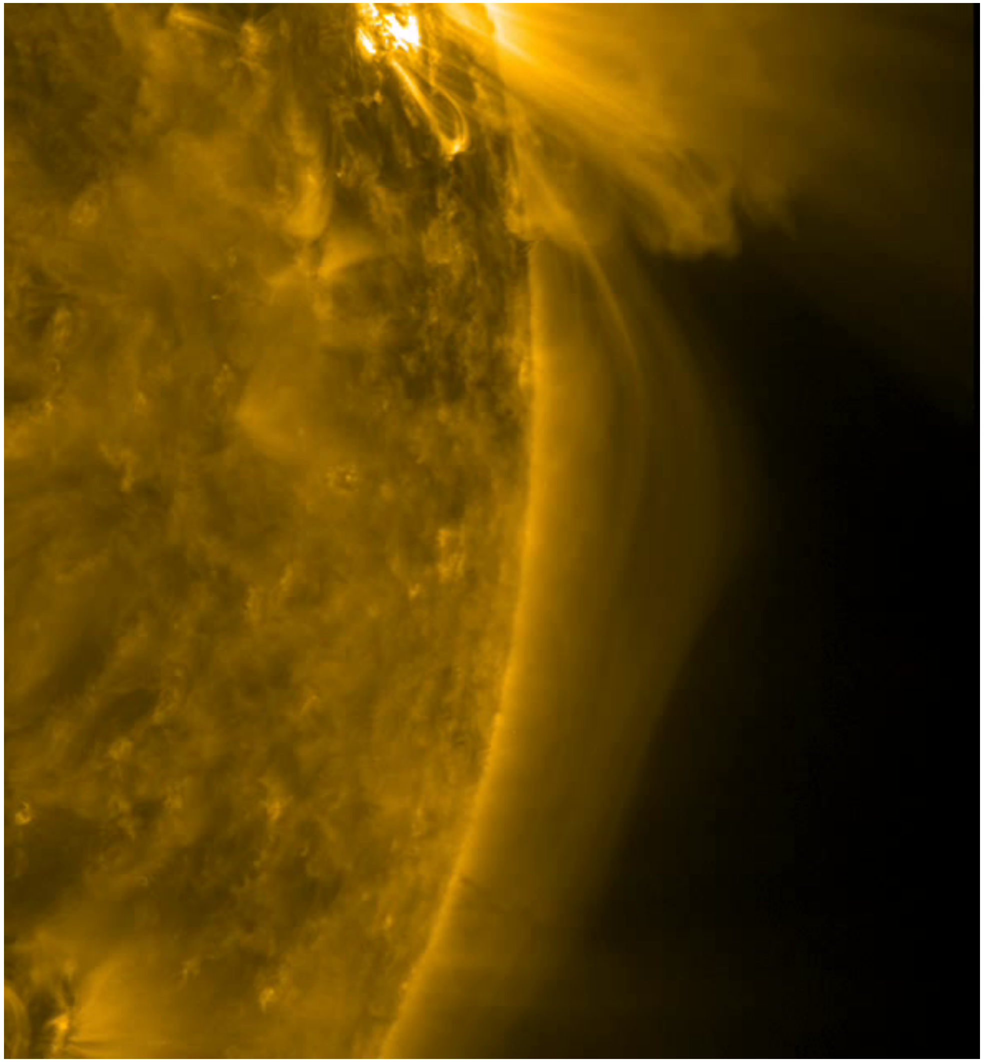

SDO/AIA 171A 2011-8-9

Modeling arcade oscillations

Ofman, Parisi, Srivasta 2015

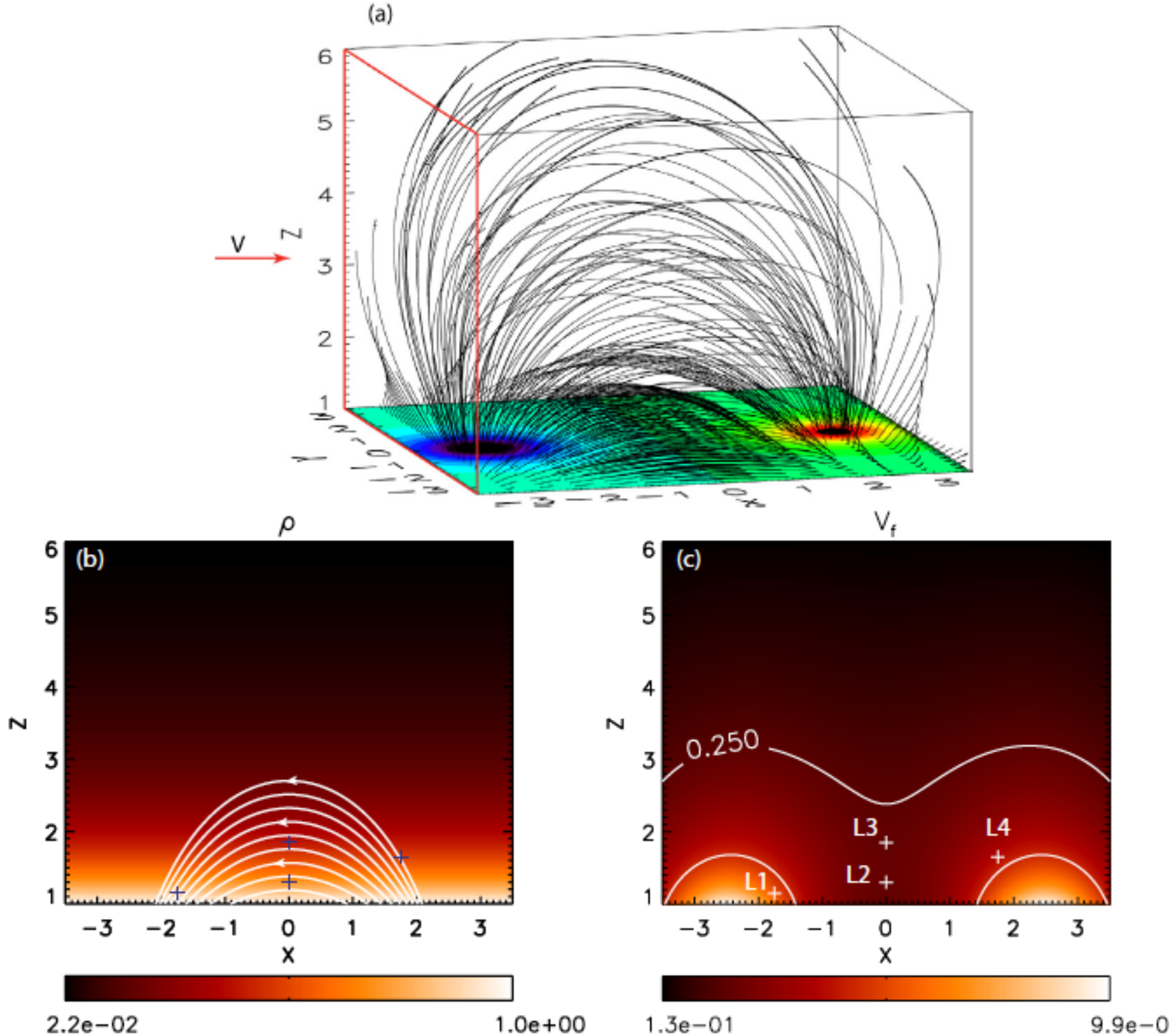

Propagation of fast MHD disturbance

Ofman, Parisi, Srivasta 2015

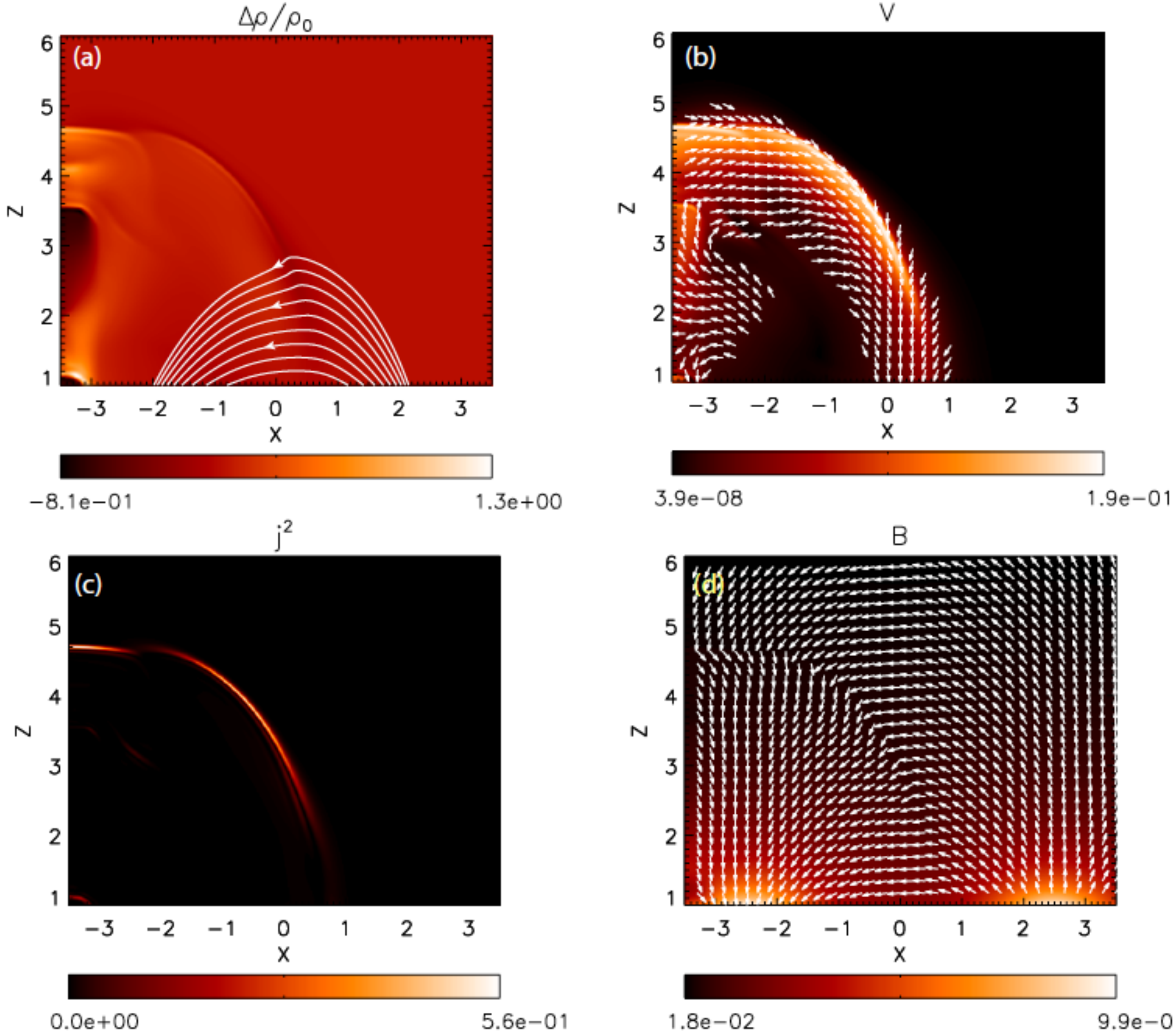

Observations vs. model

Ofman, Parizi, Srivastava 2015

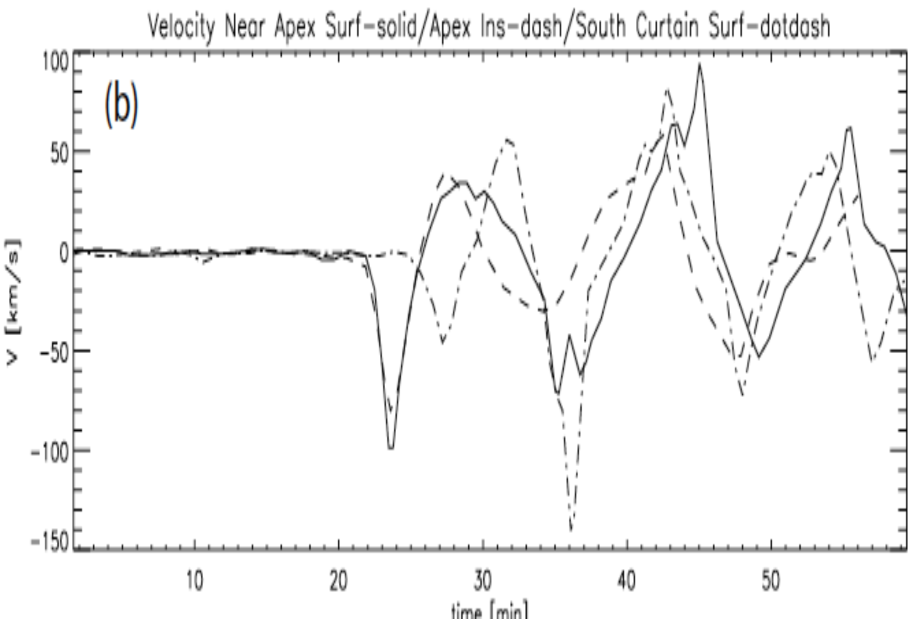

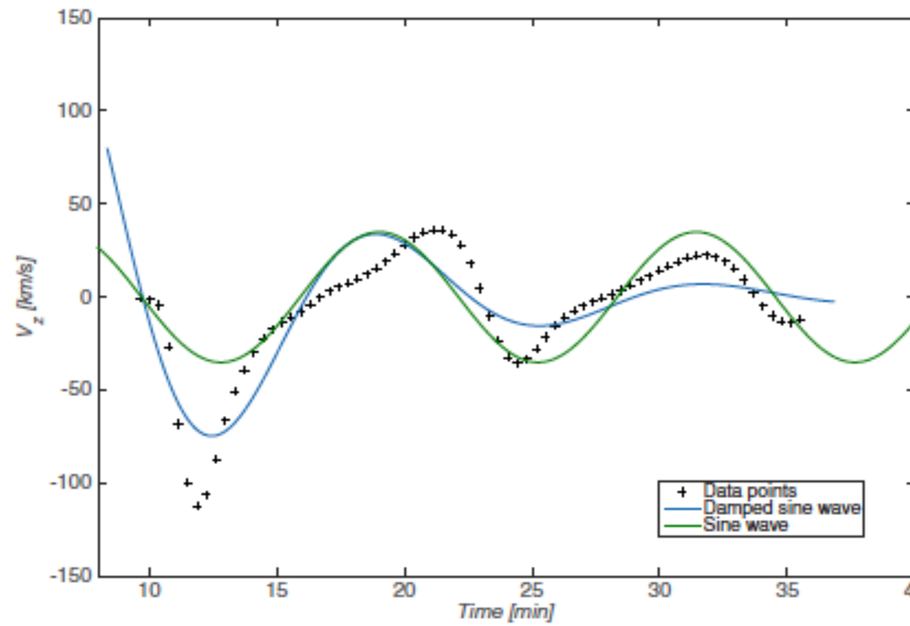

Location of observation	Observed periods [s]	MHD period [s]	B_{MHD} (G)	B_{CS} (G)
Flare Blast	530.9	565.2 ± 15.8	2.19	8.25
Apex Inside	795.8	747.9 ± 22.3	3.06	4.63
Apex Surface	896.9	885.6 ± 26.0	2.89	4.25
Southward Surface	763.8	777.6 ± 10.7	3.39	4.39

Conclusions

- Observations by SDO/AIA in EUV find quasi-periodic propagating fast (QPFs) intensity variations associated with impulsive events in active regions.
- We develop 3D MHD model of driven fast magnetosonic waves in a bipolar active region funnel in order to study these events and develop improved coronal seismology.
- We find that the modeled waves produce signatures similar to observations: the waves are propagating at the local fast magnetosonic speed and are trapped in the background 3D fast magnetosonic speed structure of the model active region.
- The results of the 3D MHD model support the interpretation of the observed waves in terms of propagating quasi-periodic weakly nonlinear fast magnetosonic waves.
- The combination of the 3D MHD model and the observations allows further development of coronal seismology, that includes magnetic, density, and temperature diagnostic, based on realistic modeling.